13th International Symposium on Turbulence and Shear Flow Phenomena (TSFP13)
Montreal, Canada, June 25–28, 2024

# DYNAMIC CHARACTERISATION OF AJVG-CONTROLLED SHOCK/BOUNDARY-LAYER INTERACTIONS ON FLEXIBLE PANELS

**Deepak Prem Ramaswamy**
Institute of Aerodynamics & Chair of Fluid Mech.
RWTH Aachen University
Wüllnerstr. 5a, 52062 Aachen, Germany
d.ramaswamy@aia.rwth-aachen.de

**Alex Storrer**
Department of Mechanical & Industrial Engg.
Northeastern University
360 Huntington Ave, 445 SN, Boston, MA 02115, USA
storrer.a@northeastern.edu

**Anne-Marie Schreyer**
Institute of Aerodynamics and Chair of Fluid Mech.
RWTH Aachen University
Wüllnerstr. 5a, 52062 Aachen, Germany
a.schreyer@aia.rwth-aachen.de

## ABSTRACT

Unsteady shock-wave/turbulent boundary layer interactions (STBLIs) are commonplace in many air and space transportation systems. They are notable for their low-frequency unsteadiness, which can compromise structural integrity. In this study, we aim to mitigate and control the detrimental aerodynamic and structural effects brought about by STBLIs over compliant surfaces using a single row of steady air-jet vortex generators (AJVGs) placed upstream of the interaction region. Both rigid and compliant walls were investigated for the baseline and AJVG-controlled compression-ramp-induced STBLIs at Mach 2.52. Measurements were performed using focusing-schlieren and digital image correlation setups, and modal reduction of the obtained spatio-temporal datasets was carried out using spectral proper orthogonal decomposition (SPOD). Results for the low-frequency unsteadiness and the panel deformation dynamics are presented and discussed both for the baseline and AJVG-controlled configurations.

## INTRODUCTION

Shock-wave / turbulent-boundary-layer interactions (STBLIs) occur in various external and internal flows in supersonic flight and propulsion systems, e.g. air-breathing engines, rocket engine nozzles, etc. When the shock wave is sufficiently strong, the boundary layer separates and detrimentally affects the aerodynamic performance. Some adverse effects of shock-induced separation include total pressure loss, inlet instabilities, and locally high pressure and thermal loading. Additionally, a low-frequency unsteadiness of the shock/separation-bubble system (see e.g. Clemens & Narayanaswamy (2014)) is particularly relevant due to the proximity to the resonant frequencies of typical aerospace structures. The resulting shock motion could thus either force unfavourable structural vibrations or cause sustained limit-cycle oscillations (LCOs), which may compromise the structural integrity by accelerating structural fatigue/failure.

Thus, reducing shock-induced separation and controlling the shock-oscillation frequency is of great interest. In this regard, mechanical sub-boundary layer micro-vortex generators and air-jet vortex generators (AJVGs) have shown promising effectiveness, albeit only on rigid surfaces (see e.g. Titchener & Babinsky (2015); Ramaswamy & Schreyer (2021, 2022*b*)).

However, modern aerospace systems increasingly utilise lightweight structures, and as a consequence, many surfaces and structures are not rigid. In such cases, the unsteady loads imposed by STBLIs result in complex fluid-structural interactions and coupled dynamics with the compliant surfaces.

While STBLIs over rigid walls have been extensively studied for different configurations over several decades (Gaitonde, 2015), the effects of flexible walls on the coupled dynamics have yet to be understood, although progress has been made (Daub *et al.*, 2016; Hoy & Bermejo-Moreno, 2021; Spottswood *et al.*, 2019; D'Aguanno *et al.*, 2023; Schreyer *et al.*, 2022). Furthermore, only limited studies exist (Schreyer *et al.*, 2022; Palakurthy *et al.*, 2024) that discuss the effects of separation control devices on the panel flutter characteristics.

In our previous studies (Ramaswamy & Schreyer, 2021, 2022*b*; Schreyer *et al.*, 2022), we investigated the general effects of separation control with AJVGs on STBLIs over both rigid surfaces and flexible surface panels. Panels of various geometries were tested with and without separation control using flow visualisations, PIV, and surface deflection measurements. We extend the analysis in the present study by performing modal decomposition on the obtained spatio-temporal dataset using spectral proper orthogonal decomposition (SPOD).

Using this tool, we aim to (a) investigate the low-frequency dynamics of STBLIs and their behaviour under separation control, (b) characterise and assess the panel dynamics due to the aforementioned low-frequency oscillation of the shock-separation-bubble system, and (c) identify modifications in these dynamics, brought about by separation control with AJVGs over such compliant surfaces.

## EXPERIMENTAL SETUP

The experiments for this investigation were carried out in the trisonic wind tunnel facility at the Institute of Aerodynamics at RWTH Aachen University. The intermittently operating in-draft facility has a stable run time of about $3-4\,\mathrm{s}$. The

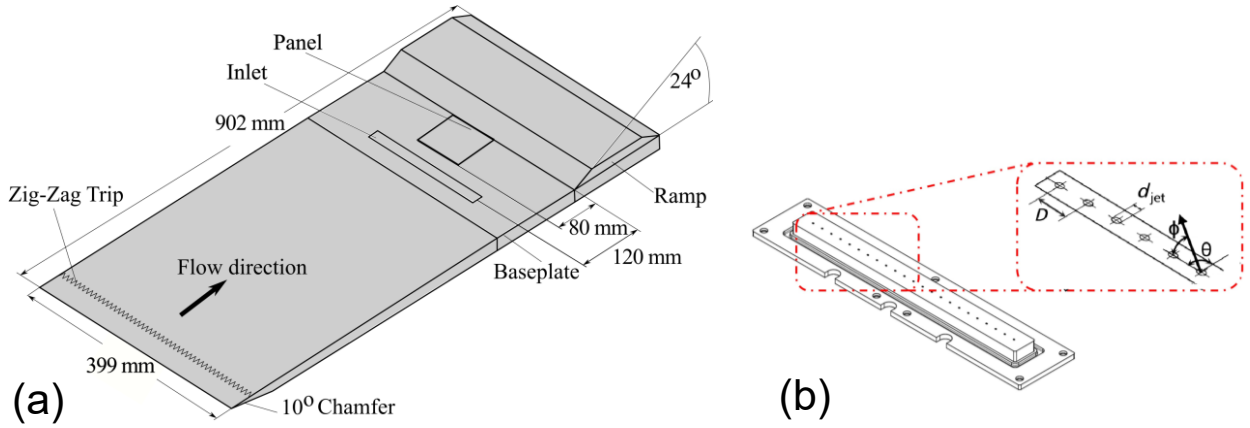


Figure 1. (a) Schematic of the compression-ramp with a flexible panel setup, and (b) detail view of the AJVG array with $D = 8d_{jet}$.

tunnel is equipped with a square test section of 0.4m × 0.4m cross-section, and optical access to the test section is provided by two circular windows on either side and one window on the top wall. The air supply to the wind tunnel is pre-dried using a silica-gel-based dryer system to prevent condensation effects; the relative air humidity was always kept well below 6%. The ambient conditions set the wind-tunnel stagnation conditions, and thus, the selected Mach number of $M_\infty = 2.52$ determines the unit Reynolds number $Re_\infty = 9.6 \times 10^6\, m^{-1}$. Table 1 summarises the main experimental conditions, where $P_o$, $T_o$ and $q_\infty$ are stagnation pressure, stagnation temperature, and free-stream dynamic pressure, respectively.

Table 1. Experimental conditions

| $M_\infty$ | $P_o$ | $T_o$ | $q_\infty$ | $\delta$ |
|---|---|---|---|---|
| 2.52 | 99.49 kPa | 297 K | 25 kPa | 10.4 mm |

A strongly separated STBLI was generated by installing a 24°-compression ramp on a flat-plate model (see Fig. 1a). The model was 902 mm long and spans the entire width of the test section. A zig-zag trip was placed close to the leading edge of the model to force transition to a turbulent boundary layer; the fully turbulent incoming boundary layer was characterised by PIV (Ramaswamy & Schreyer, 2021) and has a thickness of $\delta = 10.4$ mm at $x = 4.5\delta$ mm upstream of the ramp corner.

A cavity covered by a flexible panel was implemented into the flat-plate section of the wind-tunnel model upstream of the ramp corner, as seen in Fig. 1a. The stainless-steel panels (AISI 304) have a constant thickness of $h = 0.15$ mm and a length of $a = 80$ mm. The length was determined such that the foot of the baseline (rigid wall) separation shock approximately bisects the panel. The panel was firmly secured at both its leading and trailing edges, while the side edges can move freely; the cavity is thus not pressurised. The non-dimensional flutter parameter was calculated to be $\lambda = 509$.

For this investigation, two panel geometries were tested: (a) Flex40 - a rectangular panel with the panel width $b = 40$ mm and an aspect ratio $AR = b/a = 0.5$, and (b) Flex80 - a square panel with the panel width $b = 80$ mm and an aspect ratio $AR = b/a = 1$. The Flex40 case is similar to the panel studied by D'Aguanno *et al.* (2023) while the Flex80 is expected to clarify the effects of increasing panel aspect ratio.

Furthermore, to study the effectiveness of AJVGs in separation control, a modular inlet was designed (see Fig. 1b) and installed 120 mm (=11.5$\delta$) upstream of the ramp corner (see 1a). The AJVG array consists of a single row of 23 circular jet-orifices with jet-orifice diameter $d_{jet} = 1$ mm, jet spacing $D = 8d_{jet}$, injection angles $\phi = 45°$ and $\theta = -90°$ (see Fig. 1b). The jet injection pressure is equal to the wind tunnel stagnation pressure, and the total mass-flow rate was 0.0041 kg/s; the selected AJVG parameters have been shown to impart favourable separation-control effectiveness regarding separation length (Ramaswamy & Schreyer, 2021, 2022*b*).

The 3D deformation of the panel was measured using a time-resolved stereoscopic DIC system. For this, a speckle pattern was applied to the matte-black painted panel surface, which was continuously illuminated using off-the-shelf tungsten light sources. Images of this speckle pattern were recorded using two Photron SA.5 high-speed cameras placed on either side of the test section. The cameras were equipped with Tamron SP AF 180mm f/3.5 objectives installed using Scheimpflug mounts. The cameras recorded stereo images at 9.3 kHz with a resolution of 1024 x 640 pixels (9.8 px/mm) at an exposure time of approx. 100 $\mu$s. The recorded images were processed using Dantec DynamicStudio 6.4. The panel deflections were obtained by correlating a reference image at the rest position of the panel with that of the oscillating panel using an Adaptive PIV algorithm. For each test case, 5000 time-resolved stereo images were acquired by both cameras over a course of about 0.5 s.

Furthermore, density gradients of the rigid STBLI cases were characterised with an in-house-built focusing schlieren setup (Schauerte & Schreyer, 2018) with the focus plane at the model centreline. For this, a single Photron SA.5 high-speed camera was used to acquire images at 20 KHz with a resolution of 704px × 520px and an exposure time of approx. 2$\mu$s.

## Spectral Proper Orthogonal Decomposition

Modal decomposition of the panel deformation and the Schlieren density gradients were carried out by applying the spectral proper orthogonal decomposition algorithm (SPOD, see Towne *et al.* (2018); Schmidt & Colonius (2020)). Unlike conventional snapshot-POD, SPOD is optimal in expressing the time-resolved displacement or density fields that are coherent in both space and time and are thus suited to extract

features with a specific characteristic frequency. We applied SPOD to both the rigid panel schlieren fields and the flexible panel DIC displacement fields. Prior to processing, the datasets were truncated to the relevant field of view (FOV), background-subtracted, and a mask was applied to limit the analysis to the FOV of interest: for the Schlieren data, the mask removed the region downstream of a hypothetical Mach wave generated at the ramp-corner, and for DIC, the FOV was limited to the respective panel surfaces. The computational burden was reduced by following Welch's method and splitting the time signal into $n$ segments ($n = 39$ for Schlieren, $n = 8$ for DIC), overlapped by 50%; we thus ensured a reasonable statistical convergence and suitable frequency resolution.

## RESULTS AND DISCUSSION

This section will discuss the results of the modal decomposition of the flexible panel deformation dataset, including the spectral distribution of mode energies and their shape. Prior to this, a characterisation of the wind-tunnel model vibrations and the rigid-panel STBLI's low-frequency unsteadiness will be discussed. Both the undisturbed baseline case and the AJVG-controlled STBLI will be addressed for all cases.

### Wind-tunnel vibrations

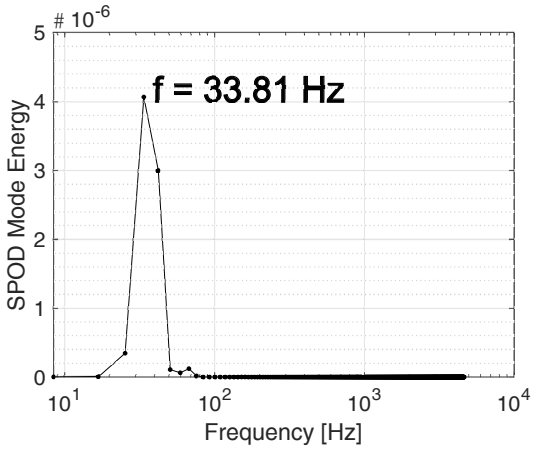


Figure 2. Spectra of the leading SPOD mode of the rigid wall oscillations

Previous studies (e.g. D'Aguanno *et al.* (2023)) have shown strong contributions of wind-tunnel vibrations on the spectral distribution of panel deformations. Therefore, to assess the influence of wind-tunnel vibrations in our current setup, DIC measurements on a rigid flat-plate section were carried out, and SPOD was applied to the measured wall-normal displacements. The results revealed a dominance of the first SPOD mode; its corresponding spectra is plotted in Fig. 2. The model oscillations show a clear peak at 33.81Hz; it agrees well with the DFFT results of oscillations at the rigid plate mid-point (38.6 Hz, see Schreyer *et al.* (2022)). The obtained dominant vibration frequency is well below the typical low-frequency unsteadiness reported in literature (Clemens & Narayanaswamy, 2014) and is thus not expected to influence the flutter mechanism induced by the STBLIs.

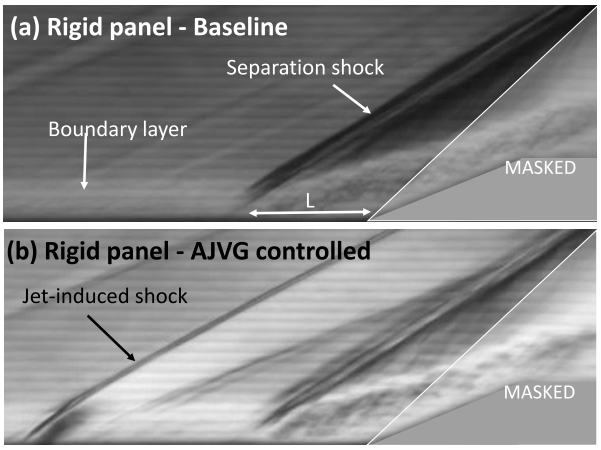


Figure 3. Focusing-schlieren images of the rigid panel: (a) Baseline and (b) AJVG-controlled. The region masked for SPOD analysis is also highlighted.

### General flow topology

In our previous study (Schreyer *et al.*, 2022), we presented a detailed investigation of the flow over rigid and flexible panels, with and without flow control, including discussions of the flow topology and the evolution of turbulence in the interaction region. Additionally, the results of panel deformation statistics were also discussed. In the following, we summarize the obtained results.

Fig. 3 shows exemplary instantaneous Schlieren images of the rigid surface cases. Typical features of the baseline (Fig. 3a) and AJVG-controlled (Fig. 3b) compression-ramp-interactions are observed: the incoming boundary layer, separation shock, jet-induced shock etc., see Ramaswamy & Schreyer (2021). Our previous study showed that both the separation length and turbulence amplification across the STBLIs increase for flexible surface panels.

The AJVG control arrays are almost equally effective on flexible panels as on rigid surfaces. However, the reduction in separation length decreases with an increase in panel aspect ratio. In general, the flow topology and flutter statistics were observed to be qualitatively similar and invariant to panel geometry and separation control.

In the following sections, we will apply SPOD to the above mentioned spatio-temporal dataset to extract dynamically dominant Schlieren and panel deformation modes.

### Low-frequency unsteadiness of rigid-wall STBLIs

Prior to characterising the panel deformation modes, it is essential to understand the behaviour of the low-frequency unsteadiness of STBLIs under the influence of flow control. For this, we performed SPOD modal decomposition on the the schlieren recordings for the rigid surface SWBLI to extract features related to the dominant low-frequency shock motion.

A previous SPOD analysis of an LES dataset of a similar configuration (Larchevêque *et al.* (2023)) has shown that the energy contributions from boundary-layer turbulence and the mixing layer dynamics are orders of magnitude larger than the locally dominant shock motion. To limit such contributions and emphasise the energy associated with the low-frequency shock motion, we masked the region downstream the ramp (see Fig. 3) before performing the SPOD decomposition.

Fig. 4 presents the cumulative pre-multiplied SPOD spectra of the first four dominant modes for both the baseline and

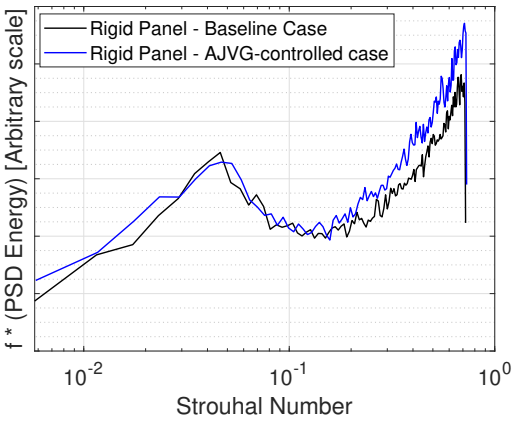


Figure 4. Cumulative SPOD spectra of the Rigid panel schlieren images over modes 1-4

AJVG-controlled configurations. A clear bump in the low-frequency domain is visible for the baseline case, with a peak frequency of $St_L = 0.0461$ (where $L$ is the length of separation, see Fig. 3). This value is slightly higher than the typical value of $St_L = 0.03$ observed from literature (Dupont *et al.*, 2006). Nevertheless, the associated mode shape (not shown here for brevity) shows a distribution dominated by the separation shock, thus confirming the mode's link to the low-frequency oscillation. The higher characteristic frequency of the low-frequency unsteadiness can be attributed to the presence of a downstream expansion corner with a favourable pressure gradient at close proximity to the mean separation bubble; a similar modification of the dynamic behaviour of the low-frequency oscillation beyond the frequency scaling associated with the size of the separation region was also reported by Larchevêque *et al.* (2023).

A similar analysis was applied to the AJVG-controlled rigid wall case, and the resulting cumulative SPOD spectra is also presented in Fig. 4. The behaviour is qualitatively very similar; the application of control thus likely does not fundamentally change the dynamics of the low-frequency unsteadiness. The corresponding peak location of the low-frequency bump is $St_L = 0.0467$. This finding is in agreement with the results and discussions of Ramaswamy & Schreyer (2022*a*), who also reported a similarity in mechanisms governing the baseline and AJVG-controlled STBLIs.

## Panel-flutter characterisation

When rigid walls are exchanged for flexible panels, the above-mentioned low-frequency shock motion induces significant panel oscillations. To determine the dominant modes of the panel, we performed an SPOD analysis of the 3D deformation data obtained from the DIC measurements.

The resulting modal spectra (not shown) reveal that dominant frequency peaks are only observed in the first mode, while the remaining modes portray minuscule spectral energy distributions. As a result, a description of only the first panel mode is presented in the following.

Fig. 5 shows the SPOD spectra of the respective first modes for the baseline and AJVG-controlled Flex40 case (rectangular AR 0.5 panel). The results show multiple clear frequency peaks for both cases. For the baseline Flex40 case, three frequency peaks are observed in Fig. 5; the corresponding mode shapes are presented in Fig. 6. A dominant frequency peak $f_1 = 185.96$ Hz ($St_L = 0.0136$) represents a typical first bending mode (see Fig. 6a) with a spanwise coherent motion in the wall-normal direction and a corresponding peak at approximately the central streamwise location.

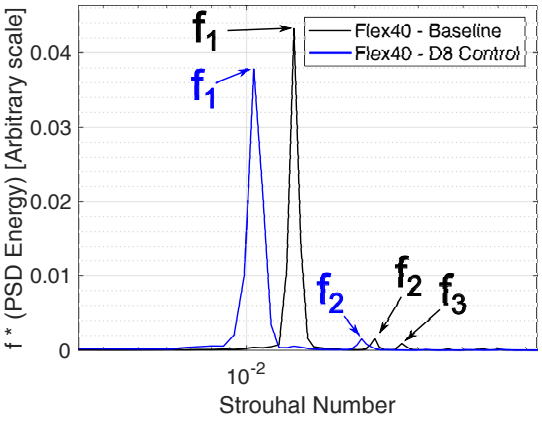


Figure 5. Modal energy spectra of the dominant mode - Baseline & AJVG-controlled Flex 40 case

The second frequency peak corresponds to $f_2 = 312.75$Hz ($St_L = 0.0228$) and represents the 1st torsional mode (see Fig. 6b); it represents alternating wall-normal movements of the edges on either side of the panel. However, the peak energy associated with this mode is 40 times lower than $f_1$.

A third minor peak is also visible in the dominant mode spectra ($f_3 = 388.82$Hz; $St_L = 0.0284$), associated with a second-order bending mode with two distinct regions oscillating alternatively (see Fig. 6c). The energy contribution is even lower; the first bending mode thus dominates the overall panel motion.

The above results for the baseline AR 0.5 panels agree well with the previous snapshot POD results from Schreyer *et al.* (2022) and D'Aguanno *et al.* (2023) for the same aspect ratio: both studies found dominant modes that are nearly 2D, and the 1st bending mode was by far the most energetic.

Fig. 5 also presents the dominant mode spectra for the AJVG-controlled case with a AR 0.5 flexible panel; the corresponding mode shapes are presented in Fig. 7. Unlike for the baseline case, only two distinct peaks are observed in the spectral distribution for the AJVG-controlled case. A dominant energy contribution occurs at $f_1 = 143.63$Hz ($St_L = 0.0105$). The mode shape corresponding to this frequency (Fig. 7a) resembles the 1st bending mode. However, the peak energy contribution is approximately 10% lower than in the baseline case for this mode.

Similarly, the second frequency bump is at $f_2 = 287.39$Hz ($St_L = 0.0210$); the corresponding mode shape (Fig. 7b) represents the 1st torsional mode with a peak energy that is approximately similar to that of the baseline case. As for the baseline case, the contribution of the 1st torsional mode to the overall energy of the panel oscillation is considerably smaller than for the 1st bending mode.

AJVGs alter the dominant oscillating frequency of the panel: under the influence of control, the 1st bending and torsional modes exhibit characteristic frequencies that are approx. 21% and 8% lower than for the baseline case, respectively. The minor contribution from the 2nd bending mode for the baseline case is absent for the AJVG-controlled case.

These results for the AR 0.5 panel demonstrate that

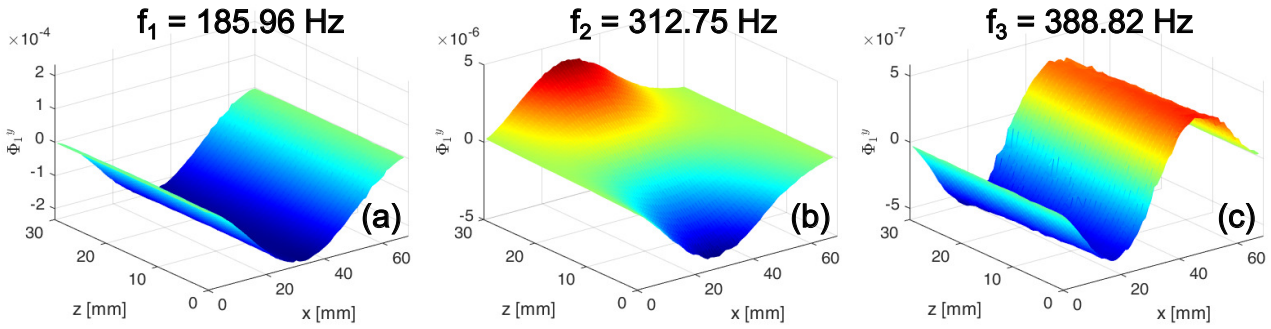


Figure 6. SPOD mode shapes of the dominant mode of the rectangular panel in the baseline configuration for three selected frequencies

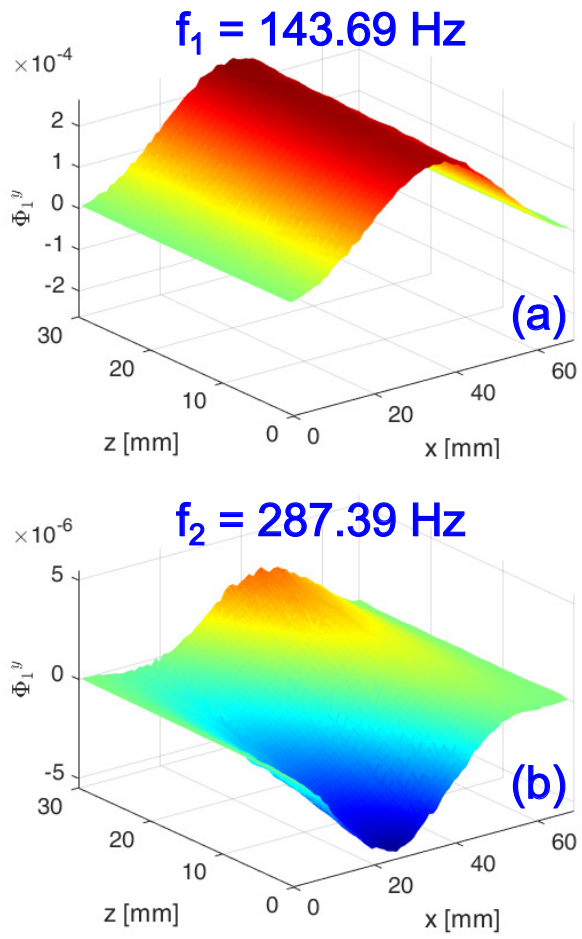


Figure 7. SPOD mode shapes of the dominant mode of the rectangular panel in the AJVG-controlled configuration for two selected frequencies

AJVGs successfully reduce the dominant panel deformation frequency, in addition to the successful reduction in separation length observed in our previous study (Schreyer *et al.*, 2022).

To analyse the influence of panel aspect ratio, we extended the SPOD analysis to the AR 1 panel with a square geometry. The associated frequencies of the resulting mode shapes for both the baseline and AJVG-controlled AR 1 case are summarised in Table 2. For completeness, the results for AR 0.5 are also included in the table.

For the baseline AR 1 case, three frequency peaks are evident, with modes corresponding to the 1st order bending ($f = 202.86\,\text{Hz}$; $St_L = 0.0146$), 2nd order bending ($f = 405.73\,\text{Hz}$; $St_L = 0.0296$) and a 2nd order torsional motion ($f = 557.88\,\text{Hz}$; $St_L = 0.0407$). As for the AR 0.5 case, the 1st-order bending mode represents the most energy (not shown). Nevertheless, the larger aspect ratio enabled the panel to also exhibit a higher-order torsional mode (at $f = 557.88\,\text{Hz}$).

With the application of control, the frequencies of both the 1st ($f = 185.96\,\text{Hz}$; $St_L = 0.0136$) and the 2nd bending ($f = 380.37\,\text{Hz}$; $St_L = 0.00278$) modes are reduced by approximately 8.3% and 6.2%, respectively. Furthermore, in addition to completely mitigating the 2nd torsional mode, the control causes the AR 1 panel to exhibit a 3rd-order bending mode at 710.03 Hz ($St_L = 0.0517$), albeit at less than 1.2% of the energy corresponding to the 1st bending mode.

On the basis of the observed dynamic behaviour of the panel, it can be expected that panels of low aspect ratios exhibit predominantly 2D dynamic behaviour, and higher-order 3D panel deflection modes are expected for panels of higher aspect ratios.

## CONCLUSIONS AND OUTLOOK

In the present experimental study, we characterised the dynamics of flexible surface panels subjected to unsteady loading by a fully separated compression-ramp-induced shock/turbulent boundary layer interaction at Mach 2.52. Both an undisturbed baseline configuration and an AJVG-controlled configuration were tested for both rigid wall and flexible wall conditions. The AJVG array was optimally configured based on previous parametric studies.

Two different flexible panel geometries were tested: an AR 0.5 rectangular panel and an AR 1 square panel. For both cases, the leading and trailing edges were firmly clamped while the side edges were freely moving. Flow measurement techniques include a focusing-schlieren setup to measure the flow density gradients and a stereoscopic DIC setup to quantify the 3D panel deformations. Modal decomposition on the obtained spatio-temporal datasets was performed using the spectral proper orthogonal decomposition (SPOD) algorithm.

Statistical analysis performed in our previous study showed that the general flow topology and the flutter behaviour are qualitatively similar for all tested cases. However, the separation length increased in the presence of flexible panels. Nevertheless, our previous study established that AJVG control mitigates shock-induced separation for all cases.

To analyze the effect of separation control on the low-freqeuncy unsteadiness of the shock/separation-bubble system, the Schlieren images of the rigid wall STBLI were decomposed using SPOD. The resulting cumulative SPOD spec-

Table 2. Dominant frequencies of the different mode shapes [in Hz]

| Case \ Mode | | 1st Bending | 1st Torsional | 2nd Bending | 2nd Torsional | 3rd Bending |
|---|---|---|---|---|---|---|
| Baseline | AR 0.5 panel | 185.96 Hz | 312.75 Hz | 388.82 Hz | - | - |
| | AR 1 panel | 202.86 Hz | - | 405.73 Hz | 557.88 Hz | - |
| AJVG Control | AR 0.5 panel | 143.68 Hz | 287.39 Hz | - | - | - |
| | AR 1 panel | 185.96 Hz | - | 380.37 Hz | | 710.03 Hz |

tra of the first four SPOD modes revealed a peak in the low-frequency domain with a separation length-based Strouhal number of $St_L = 0.0046$. The characteristic low-frequency behaviour remains largely unchanged with AJVG control, which also peaked at approximately the same location.

We then addressed the dynamic panel-deformation characteristics. Modal decomposition of the DIC data of the narrow AR 0.5 flexible panel revealed a dominant 1st bending mode for both the baseline and AJVG-controlled STBLIs. Nevertheless, the frequency associated with this mode showed a strong 21% reduction for the AJVG-controlled case. A relatively smaller reduction in peak frequency value of about 8% was identified for the 1st torsional mode that characterises the baseline and AJVG-controlled cases. For the AR 0.5 panel, a higher order 2nd bending mode that was observed in the baseline case is completely mitigated by AJVG control.

A similar analysis of the wider AR 1 flexible panel also revealed the dominant 1st-order bending mode, whose frequency is diminished by about 8.3% by AJVG control. Additionally, the wider AR 1 panel showed increased three-dimensionality: the baseline case exhibited 2nd order bending and torsional modes, and the AJVG-controlled AR1 case exhibited a 2nd order bending mode (with a 6.2% lower peak frequency in comparison to the baseline case) and a unique 3rd order bending mode, albeit at a significantly lower energy contribution.

In a future study, this analysis will be extended to higher aspect ratio panels to comprehensively understand the influence of aspect ratio. The obtained insights will allow for the development of effective control setups that will simultaneously mitigate the shock-induced separation and the associated unfavourable panel deformations, thereby alleviating threats to the structural integrity of high-speed aerospace systems.

## Acknowledgements

This research was funded by the German Research Foundation (DFG) in the framework of the Emmy Noether grant "Separation Control with Air Jet Vortex Generator Arrays in Transonic and Supersonic Flow" (No. 326485414). The second author would also like to acknowledge the DAAD-RISE program for funding his stay at RWTH Aachen University.

## REFERENCES

Clemens, N. T. & Narayanaswamy, V. 2014 Low-frequency unsteadiness of shock wave/turbulent boundary layer interactions. *Annual Review of Fluid Mechanics* **46**, 469–492.

Daub, D., Willems, S. & Gülhan, A. 2016 Experiments on the interaction of a fast-moving shock with an elastic panel. *AIAA Journal* **54** (2), 670–678.

Dupont, P., Haddad, C. & Devieve, J. F. 2006 Space and time organization in a shock-induced separated boundary layer. *Journal of Fluid Mechanics* **559**, 255.

D'Aguanno, A., Quesada Allerhand, P., Schrijer, F. F. J. & van Oudheusden, B. W. 2023 Characterization of shock-induced panel flutter with simultaneous use of dic and piv. *Experiments in Fluids* **64** (1).

Gaitonde, D. V. 2015 Progress in shock wave/boundary layer interactions. *Progress in Aerospace Sciences* **72**, 80–99.

Hoy, J. F. & Bermejo-Moreno, I. 2021 Numerical study of STBLI on flexible panels with wall-modeled LES. In *AIAA Scitech Forum*.

Larchevêque, L., Ramaswamy, D. P. & Schreyer, A.-M. 2023 Effects of favourable downstream pressure gradients on separated shock-wave/boundary-layer interactions. *International Journal of Heat and Fluid Flow* **102**, 109164.

Palakurthy, S., Zope, A., Yan, Y., Collins, E. & Bhushan, S. 2024 Numerical study of the effect of micro vortices on chaotic flutter. *Journal of Computational and Applied Mathematics* **436**, 115401.

Ramaswamy, D.P & Schreyer, A.-M. 2022*a* Unsteady flow organisation of shock-wave/boundary-layer interactions controlled with air-jet vortex generators. In *AIAA SCITECH 2022 Forum*. American Institute of Aeronautics and Astronautics.

Ramaswamy, D. P. & Schreyer, A.-M. 2021 Control of shock-induced separation of a turbulent boundary layer using air-jet vortex generators. *AIAA Journal* **59** (3), 927–939.

Ramaswamy, D. P. & Schreyer, A.-M. 2022*b* Effects of jet-to-jet spacing of air-jet vortex generators in shock-induced flow-separation control. *Flow, Turbulence and Combustion* **109** (1), 35–64.

Schauerte, C. & Schreyer, A.-M. 2018 Design of a high-speed focusing schlieren system for complex three-dimensional flows. In *Proceedings of the 5th International Conference on Experimental Fluid Mechanics*, pp. 232–237.

Schmidt, O.T. & Colonius, T. 2020 Guide to spectral proper orthogonal decomposition. *AIAA Journal* **58** (3), 1023–1033.

Schreyer, A-.M., Ramaswamy, D.P. & Schauerte, C.J. 2022 Separation control with air-jet vortex generators of shock/boundary-layer interactions on flexible panels. In *12th International Symposium on Turbulence and Shear Flow Phenomena, Osaka, Japan.*.

Spottswood, S. M., Beberniss, T. J., Eason, T. G., Perez, R. A., Donbar, J. M., Ehrhardt, D. A. & Riley, Z. B. 2019 Exploring the response of a thin, flexible panel to shock-turbulent boundary-layer interactions. *Journal of Sound and Vibration* **443**, 74–89.

Titchener, N. & Babinsky, H. 2015 A review of the use of vortex generators for mitigating shock-induced separation. *Shock Waves* **25** (5), 473–494.

Towne, A., Schmidt, O. T. & Colonius, T. 2018 Spectral proper orthogonal decomposition and its relationship to dynamic mode decomposition and resolvent analysis. *Journal of Fluid Mechanics* **847**, 821–867.